Simulation of extensional clay fractures

A. Malthe-Sørenssen, T. Walmann, J. Feder, T. Jøssang, and P. Meakin
Department of Physics, University of Oslo, P.O.B. 1048 Blindern, N-0316 Oslo, Norway

H. H. Hardy
Conoco Incorporated, P.O. Box 1267, Ponca City, Oklahoma 74603

(Received 18 June 1998)

A spring network model has been used to study fractures in thin layers of material supported by a deformable substrate. The interactions with the substrate localize the stress/strain field in the material. The crossover of the shape of a single fracture in an ordered material from an elliptical form to a long, thin shape was studied as a function of the substrate attachment strength. For many interacting fractures in a disordered material, the simulated fracture patterns reproduced the most important visual and statistical properties of fracture patterns from recent experiments on thin slabs of clay attached to a deformable substrate. In particular, the correspondence was good for a new set of scaling relations between the lengths and areas of fractures. The shapes of the larger cracks were consistent with a self-affine curve with a Hurst exponent of 0.5. The dynamics of the development of the fracture pattern corresponds qualitatively to experimental results.
[S1063-651X(98)10811-5]

PACS number(s): 64.60.−i, 62.20.Mk, 61.43.−j, 81.40.Np

I. INTRODUCTION

Fractures and fracture surfaces in disordered materials have recently received much attention. In particular, it has been argued that fracture surfaces are self-affine [1–5], and that the Hurst exponent has a universal, material independent value [5,6]. Even so, attempts have also been made to correlate the Hurst exponent with material properties such as toughness [4,6]. In some systems, many fractures are nucleated throughout the material, and the interactions between them play an important role in the material failure process. Fractures grow both by propagation at their ends and by the coalescence of smaller fractures. The growth of any individual fracture is strongly influenced by interactions with its neighbors, mediated by the stress/strain field. Systems of interacting fractures provide us with an opportunity to study properties other than the shapes of individual fractures. For example, the distribution of the shapes and sizes of the fractures can be studied, and these distributions might also have universal characteristics. In several important applications, such as the characterization and modeling of oil reservoirs, aquifers and waste storage facilities, an understanding of the distributions of fracture sizes and shapes is required, as is the way in which the fractures are organized to form a fracture network that can transport fluids through the fractured material.

In many cases of interest, fractures appear in layers of material with a large length to depth ratio that are supported and deformed by underlying (and/or overlying) layers of deformable material substrate. Familiar examples include a thin film of paint on wood, plastic or metal, a layer of dried mud on the bottom of a dried up lake (dessication fractures) or a layer of rock in the Earth's crust. In these systems, the evolution of the stress/strain field in the material is dominated by the boundary conditions for the attachment, since the stress fields are strongly localized by the attachment to the substrate. However, the propagation of any individual fracture is still influenced by its neighbors because the presence of a fracture changes the stress/strain field in its vicinity. This type of boundary condition is not only an integral part of a wide range of natural systems, but it also greatly simplifies the problem from a computational point of view, because of the effect of the growth of one crack tip is localized and does not necessarily change the *entire* stress/strain field after each growth event.

A typical example of such a system is a thin slab of clay that has been prepared on a deformable substrate. Clay models have been used to study large scale geological processes on laboratory scales for almost 200 years [7–11]. The use of clay models for this purpose is based on classical scaling theory [12] and the rheological similarity between clay and the Earth's crust. A recent series of experiments [13] has shown that the fracture patterns formed during extensional deformation of supported layers of clay were characterized in terms of a scaling relation between the fracture length L and the open fracture area A, $L \propto A^{\beta}$. The exponent β was found to be approximately the same for both experiments and simulations. The study focused on extensional deformations since the fractures and faults open during extensions and the fracture pattern could therefore be easily visualized. Extensional deformations are also frequently dominant in oil reservoirs and these scaling relations may therefore have technological relevance. Here, the model presented in [13] is studied in more detail, with emphasis on the statistical properties of fracture patterns and individual fractures, and the dynamics of the fracturing process.

Several models have been proposed to simulate fracture processes in two-dimensional systems. For example, molecular dynamics models have been applied to simulate atomic fracture dynamics [14,15]. However, these models are restricted to systems of very small size. Models inspired by statistical physics and disordered systems in particular have been more successful in describing macroscopic behavior. In these models, the system is represented by a network of

simple mechanical units that represent the properties of the material averaged over an intermediate scale between the overall macroscopic scale of the material and the scale of microscopic details such as the size of the clay particles. For example, a two-dimensional material can be represented as a lattice of interconnected springs. The inherent disorder in the material can be quenched (each material element is given material properties selected randomly from some distribution that is characteristic of the model) or annealed disorder can be introduced by removing or modifying mechanical elements in the network randomly, with probabilities that depend on both the properties of the individual mechanical elements and the local stress/strain conditions that they are subjected to. In this case, fracturing is represented by breaking material elements irreversibly, and removing them from the lattice. Models have also been developed in which the mechanical elements are beams that can locally sustain shear [16,17]. Also, a scalar, electrical analog of the spring network model [18–20], called the random fuse model, has been used widely to study the fundamental aspects of fracture [20–23].

Most studies carried out using mechanical network models have been limited to small system sizes because of the long range effect of breaking a single bond. The Laplace equation (for random fuse models) or linear elasticity equations must be solved after each bond is broken and the computational cost of solving such equations increases rapidly with system size. Meakin [24] developed a ''substrate supported'' model in which a two-dimensional spring network was bound to a substrate using elastic springs. If the modulus of the springs connecting the network to the substrate is not too small relative to the moduli of the springs in the two-dimensional network, the perturbation of the system resulting from the removal of a single bond is localized and calculations can be sped up significantly. The electrical (scalar) analog of the substrate supported model was developed by Colina *et al.* [25] who suggested that it could be used to simulate the drying of clay. However no quantitative comparison between the model results and natural or laboratory cracking patterns was made.

In this article, we study the fracturing in a large elastic network attached to a deformable substrate and attempt to make a direct comparison with recent experiments on fractures in clay. Comparisons are made visually and by using statistical measures of the fracture pattern, such as the size distribution of fractures and a proposed scaling relation between fracture length and area. This article is divided in two parts. The first part addresses the behavior of a single fracture in an ordered material. This allows a detailed study of the effect of the substrate attachment on the fracture shape and the propagation of the stress field. Since there are no corresponding experimental studies on clay, the results were compared with elliptical fractures described by linear elasticity theory [26]. In particular, the scaling relation $L \propto A^{\beta}$ is studied for the growth of a single fracture. The second part of this article discusses the behavior of a disordered material subjected to uniform extension. In this case, a pattern of interacting fractures is generated. The distribution of shapes and sizes of the fractures is studied and compared with the patterns from clay. The simulated patterns reproduce the most important visual and statistical properties of the experimental clay patterns. In addition, the self-affine scaling properties of individual fracture and the time development of the fracture pattern were studied and compared to experimental data. The simulation model used both for studies of a single fracture in an ordered material and of many fractures in a disordered material, is presented in Sec. II. Section III discusses the behavior of a single fracture, and Sec. IV addresses the behavior of materials with many fractures. The results are discussed and compared with experiments in Sec. V. Finally, conclusions and suggestions for further study are presented in Sec. VI.

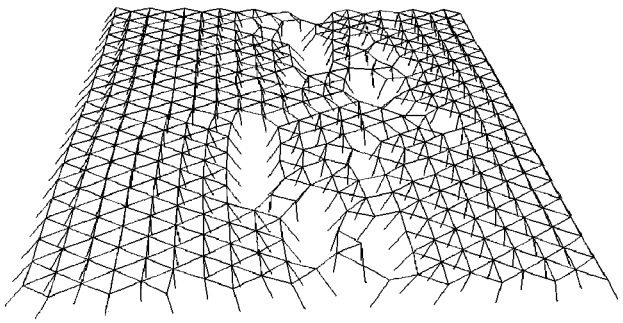

FIG. 1. The material is represented by a triangular lattice of springs, each with spring constant κ and equilibrium length l. Each node is connected to an underlying substrate with a spring of zero equilibrium length and spring constant κ_0. In the model, the nodes and the substrate attachment points are in the same plane. The elastic network and substrate attachment planes have been separated in this figure to show the connecting springs.

II. SIMULATION MODEL

The material is modeled as a network of simple mechanical units, as explained above. Here, a triangular network of interconnected springs represents the material. Fracturing occurs through the irreversible removal of a spring if the stress in the spring exceeds a threshold value. The material properties of the material are determined by the properties of the springs and the breaking thresholds. The springs are assumed to be Hookean (the force is linear in the elongation) and the equilibrium length and spring constants of the springs are constant. The boundary interactions are reduced to a simple set of boundary conditions: The surface layer of springs is attached to a deformable substrate representing either a single substrate or a pair of substrates that lie above and below the deformed material. The coupling is through weak springs attaching each node to the substrate as illustrated by Fig. 1. The deformation of the layer is controlled by the motion of the substrate and the substrate spring attachment points. The net force acting on a node i at a position $\vec{x}_i'$ is

$$\vec{f}_i = \sum_{\langle i,j \rangle} \kappa_1 (|\vec{x}_i' - \vec{x}_j'| - l)\vec{u}_{i,j} + \kappa_0 (\vec{x}_{0,i}' - \vec{x}_i'), \qquad (1)$$

where the sum is over all connected neighbors j, $\vec{u}_{i,j}$ is a unit vector from j to i, $\vec{x}_{0,i}'$ is the position of the substrate attachment points for node i, l is the equilibrium distance between node i and j, κ is the spring constant, and κ_0 is the substrate spring attachment constant. The equation can be

simplified through a normalization with the spring constant and the equilibrium length. The resulting equation is

$$\frac{1}{\kappa l}\vec{f}_i=\sum_{\langle i,j\rangle}(|\vec{x}_i-\vec{x}_j|-1)\vec{u}_{i,j}+k(\vec{x}_{0,i}-\vec{x}_i), \tag{2}$$

where $\vec{x}=\vec{x}'/l$ and the effective substrate attachment spring constant, $k=\kappa_0/\kappa$, is the ratio of the substrate spring constant and the internode spring constant.

During a simulation, the material is deformed by deforming the substrate and moving the substrate attachment points in small steps. After each step, the spring network is relaxed so that the energy is at a minimum or, equivalently, so that the net force on all nodes is zero. A bond can only sustain a certain stress and breaks if the stress exceeds the breaking threshold. If any spring exceeds its breaking threshold, it is removed from the network, and the network is relaxed again. This procedure is repeated until no more bonds break. The substrate is then deformed one further step and the relaxation repeated.

Standard overrelaxation techniques [27] were used to reach a new mechanical equilibrium after each spring rupture event. The relaxation is characterized by the relaxation threshold ϵ. Only nodes that would move further than ϵ in a relaxation step were actually moved during the relaxation cycle. The attachment to the substrate strongly localize the perturbations from a bond rupture. In view of this localization the relaxation was intensified in the regions around the fracture tips during each relaxation cycle. This method greatly reduced the calculation time.

The effective substrate attachment force constant, k, introduces a characteristic length scale λ in the model. The attachment inhibits propagation of the stress field. It can be shown that a perturbation from a bond rupture decays exponentially in one dimension [25,28] and for small k the average length between neighboring fractures, λ, scales as $\lambda \propto 1/\sqrt{k}$ in one dimension. The two-dimensional case of pure extension is expected to behave similarly: A fracture will relax the nodes close to its sides, but the relaxation is exponentially localized. After a length λ the stress will be similar to that in an unfractured lattice.

In the substrate attachment model, the relaxation threshold ϵ is chosen so that $\epsilon \ll k$. However, the physical interpretation of ϵ can be illustrated by examining the case in which $\epsilon \gg k$. In this case, the relaxation in the network is dominated by ϵ and not by k. During each relaxation event, each node is displaced by a distance proportional to the net force acting on it, and for small k, this is approximately proportional to the forces from the connected nodes in the layer. Nodes on which the force is smaller than the threshold, ϵ, will not be moved, corresponding to the effect of a static friction force acting on all nodes. In this limit, the model can be described as a network of interconnected blocks that rest on the substrate. During extension, all the blocks are moved with the substrate. Then the network is relaxed, and a static friction with a threshold proportional to ϵ is imposed on each block from the substrate. The model is therefore analogous to a spring-block model on a triangular lattice. Results obtained from the spring-block model will be discussed and compared to the substrate attachment model.

The deformation in both models is determined by the motion of the substrate attachment points. Each point can be moved individually, allowing many different types of deformations to be implemented. Here, we will study extensional deformations only, and leave other modes of deformation for a further study. For a uniform extension in the y direction, the displacement of the substrate nodes at a total extension t is

$$\vec{x}_{0,i}(t)=\begin{bmatrix}1 & 0\\ 0 & 1+t\end{bmatrix}\vec{x}_{0,i}(t=0). \tag{3}$$

Periodic boundary conditions are applied in both the x and the y directions in order to reduce finite size effects. Periodic boundaries can be a problem for long fractures that propagate across the sample, since the fracture will screen itself. However, the simulations were stopped at small deformations to eliminate such difficulties.

III. SINGLE FRACTURE IN AN ORDERED MATERIAL

The behavior of a material consisting of a network of interconnected springs can be described by linear elasticity theory [23] when boundary conditions are imposed on the edges only. However, for the substrate attachment model and the spring-block model, the boundary conditions and the imposed stress differ from the classical picture with stresses applied only at the edges of the network. In order to study the effect of the substrate attachment, a simple case of fracturing was studied for the models and compared with results from linear elasticity theory. A particularly simple case of fracturing, for which similar solutions from linear elasticity theory are known, is the growth of a single fracture in an ordered material far from the edges of the network.

In fracture theory for elastic materials, an elliptical fracture far from the boundaries in a two-dimensional material with a uniform extensional stress is described by the length of the elliptic half-axes a and b. The width of the fracture, $w(x)$, a function of the distance, x, to the fracture tip, increases from 0 to $w_{\max}=b$:

$$w(x)=w_{\max}\sqrt{\frac{x}{a}}\left(2-\frac{x}{a}\right)^{1/2}. \tag{4}$$

For an elastic material, the maximum width is proportional to the fracture length $L=2a$: $w_{\max}\propto L$ [26]. Close to the fracture tip, the width is approximately proportional to the square root of the distance from the tip:

$$w(x)\simeq w_{\max}\left(\frac{x}{a}\right)^{1/2} \quad \text{for } x\ll a. \tag{5}$$

According to linear elasticity fracture mechanics, the stress σ_{xx} decays as a power-law away from the tip of an elliptical fracture according to $\sigma_{xx}=C(a/x)^{1/2}$.

The simulation model differs from the ideal case described by fracture mechanics in several respects. The model is discrete and the fracture has a smallest scale given by the lattice size. A fracture in the simulation model is therefore not a purely elliptical fracture. The loading conditions are also very different in the simulation model, since stress is

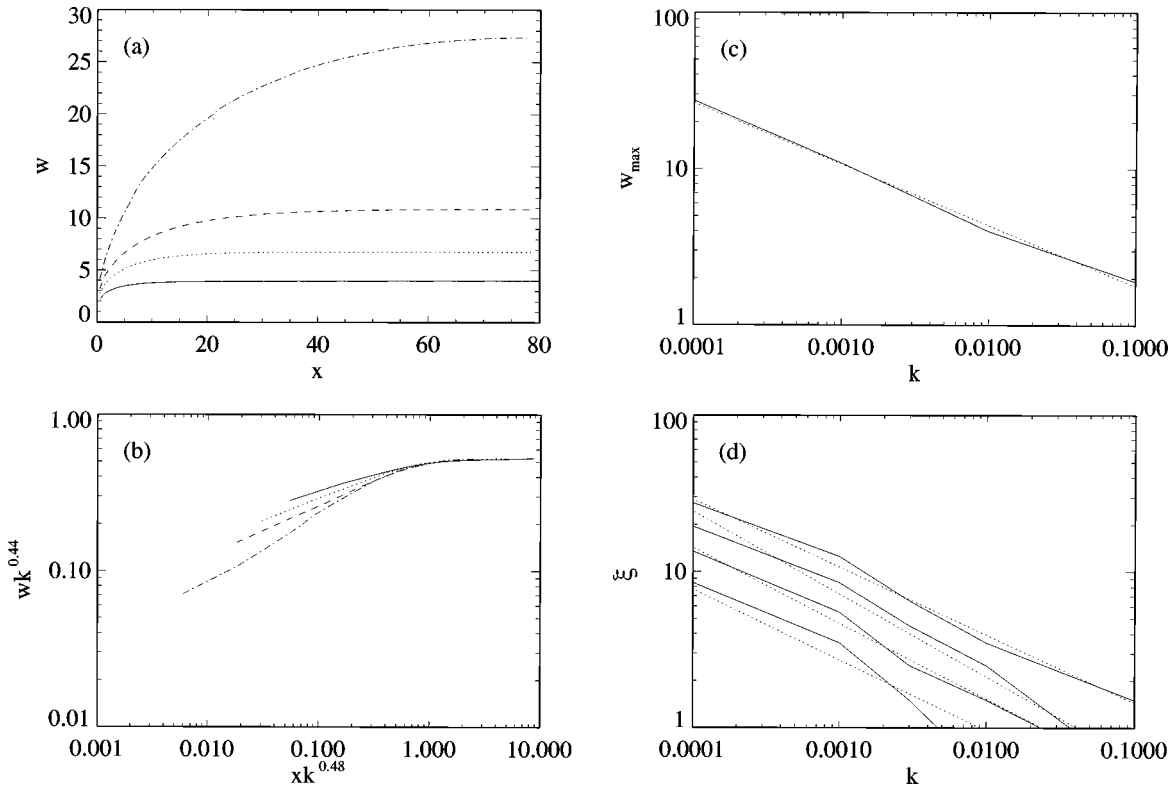

FIG. 2. Part (a) shows plots of the width of the fracture $w(x;k)$ as a function of x, the distance from the fracture tip, and k, the substrate attachment spring constant. The different curves are (from bottom to top) for $k=10^{-2}$, 3×10^{-3}, 10^{-3}, and 10^{-4}. The curves cross over from power-law behavior for small x to a flat plateau for large x. Part (b) shows a data collapse plot based on the scaling form $w(x;k)=k^{-\beta_w}g_w(xk^{-\nu_w})$. Part (c) shows a plot of the function $w_{\max}(k)$, which indicates that it has a power-law form. Part (d) show plots of ξ_w as a function of k, where ξ_w is determined from $w(\xi_w;k)=zw_{\max}$. The curves shown are for $z=0.9$, 0.8, 0.7, and 0.6 (from top to bottom).

applied to all nodes through the substrate attachment. A single fracture was prepared in the simulation model for comparison with the theoretical results. All the springs in the triangular network were given identical material properties: the equilibrium length and the spring constants were the same for all nodes. A uniform stress corresponding to an extension t of the substrate was imposed on the system. Initially, the center bond was removed. The fracture was grown without changing the imposed stress by repeatedly breaking the most strained bond along the border of the fracture, creating an open, connected region. The simulation model used here therefore differed from the earlier description, since the substrate was fixed at a given extension, t, and a fracture was grown according to specific rules irrespective of breaking thresholds. However, these changes allow the effect of the substrate attachment to be studied for a single fracture. Simulations were performed for both the substrate attachment model and the spring-block model, and the parameters k and ϵ were varied systematically. Simulations were also performed for different spring network sizes, Λ, measured in units of equilibrium bond lengths. The results for the substrate attachment model are discussed first.

The simulated fracture was characterized by the width $w(x)$ as a function of the distance x to the fracture tip. Figure 2(a) shows the behavior of $w(x,k)$ for different values of k for $\epsilon=k/300$ on a 400×400 lattice. Close to the fracture tip the width increases rapidly with x. The behavior is consistent with a power law $w\sim x^{1/2}$, which is similar to the theoretical result for a continuum elastic medium. For large x, the width approaches a constant $w_{\max}$. The behavior of the width can therefore be characterized as a crossover from a power-law form to a constant function at a crossover length ξ_w. For $x\ll\xi_w$, the width is approximately a power law, and for $x\gg\xi_w$, the width is constant. Both the maximum width $w_{\max}$ and the crossover length ξ_w vary systematically with k. Similar crossovers are frequently observed in other areas of statistical physics, for example, in percolation theory [29]. Mapping the crossover behavior is often a useful tool in understanding the functional dependence of the characteristic lengths on the parameters that are varied systematically. Based on ideas from crossover analysis, we propose the simple scaling form

$$w(x,k)=k^{-\beta_w}g_w(xk^{-\nu_w}) \tag{6}$$

for the width, where the function $g_w(u)$ is a crossover function, which is a power law for small u and constant for large u:

$$g_w(u)=\begin{cases} c_1u^{\alpha_w} & u\ll u_0 \\ c_2 & u\gg u_0 \end{cases} \tag{7}$$

Figure 2(b) shows the best data collapse for the fracture width. The data collapse is not very good; there are clear discrepancies for small lengths. However, the collapse appears to characterize both the behavior of the maximum width and the crossover length sufficiently well. The exponents found from the data collapse indicate that $\xi_w\propto k^{\nu_w}$,

where $\nu_w = -0.48 \pm 0.05$, and $w_{\max} \propto k^{-\beta_w}$, where $\beta_w = 0.45 \pm 0.05$. This exact behavior was, however, anticipated, since the localization of stress perturbations due to the substrate attachment implies the following physical picture: The substrate attachment introduces a length scale λ, which describes the exponential decay of perturbations in the stress field. For a one-dimensional model, λ depends on the substrate attachment spring constant k, $\lambda \propto k^{-1/2}$. At length scales sufficiently smaller than λ, the model is not influenced by the substrate attachment and behaves as an unattached spring network with a constant, imposed stress. This is the exact situation described above for elliptical fractures in linear elasticity theory. At lengths much greater than λ, the behavior is dominated by localization, which prevents the fracture from widening when it grows at an end. Consequently, in the limit of large lengths the fracture grows in length with a constant width. The power-law form of the characteristic length, ξ_w, and the values of the power-law exponents found above, are consistent with this picture. At distances significantly smaller than the characteristic length, the power-law behavior $w \sim x^{1/2}$ is observed, as expected theoretically for elliptical fractures. The length ξ_w separates the two behaviors and corresponds to λ. The power-law dependence on k is also the same (within the uncertainties) for ξ_w and λ. Similarly, the maximum width $w_{\max}$ is also approximately proportional to λ. The only relevant length scale in the system is therefore the localization length, λ. This implies that

$$w(x,k) = \lambda g_w'(x/\lambda) = k^{-1/2} g_w(x k^{-1/2}), \tag{8}$$

where $g_w'(z) \propto g_w(z)$, and that the exponents β_w and ν_w have values of 1/2 and $-1/2$, respectively. The values of $\beta_w = 0.45 \pm 0.05$ and $\nu_w = -0.48 \pm 0.05$ are consistent with these simple theoretical predictions.

The data collapse for $w(x,k)$ is rather poor. Several factors influence the behavior of w. For small lengths, the finite lattice size affect the results, and the dynamic range of values for the width, the span between the smallest and the largest value, is narrow. Due to these factors, the uncertainties are large. However, the scaling results proposed above were also tested directly. The maximum width $w_{\max}$ was measured directly as a function of k, as shown in Fig. 2(c). The behavior is a reasonable power law, and the best fit gives the relation $w_{\max} \propto k^{-0.4 \pm 0.1}$. The maximum width is therefore, within the uncertainties, proportional to λ. Similarly, the characteristic length ξ_w was measured directly. A reasonable definition of the characteristic length is the length ξ at which the width had reached a fraction z of its maximum value: $w(\xi;k) = z w_{\max}$. Figure 2(d) shows a plot of ξ as a function of k for several values of z. The dependence is again approximately a power law, $\xi_w \propto k^{0.48 \pm 0.1}$, which indicates that the characteristic length is proportional to λ. Consequently, the results from the data collapse are valid, even though there are obvious deviations from the scaling form given in Eq. (6).

For an elliptical fracture, the fracture shape is characterized by the ratio between the fracture width $w_{\max}$ and length L. A more precise measure, which takes into account the variation of the width along the fracture, is the average width $\langle w \rangle$, averaged along the length of the fracture. Equivalently, the shape can be characterized by the fracture length and area

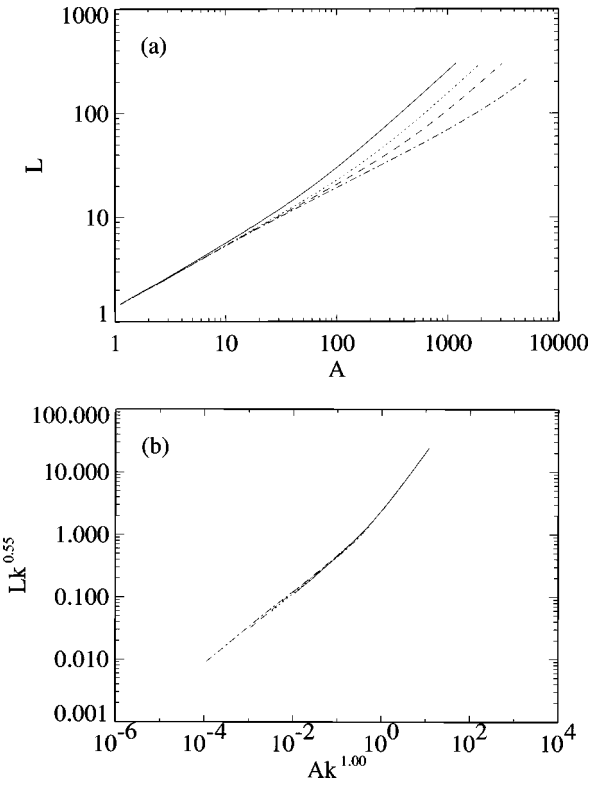

FIG. 3. A plot of the length $L(A;k)$ as a function of the fracture area A and substrate attachment force constant k. Part (a) contains a direct plot and (b) shows a data collapse plot for $k = 10^{-1}, 10^{-2}, 3 \times 10^{-3}, 10^{-3}, 10^{-4}$.

A since the average width is defined as $\langle w \rangle = A/L$. A similar measure has been proposed to characterize the statistical properties of fracture patterns, and it is therefore interesting to study the growth of the length and area during the growth of a single fracture, in order to compare with that of a fracture pattern. Figure 3(a) shows a plot of the length L as a function of the fracture area A obtained from the simulation of a single fracture in an ordered material. Both fracture length and area grow when the fracture grows, and the curve shows the relation between the two. The curve displays a clear crossover that varies systematically with the substrate attachment spring constant, k. Based on the ideas presented above, a data collapse of the form

$$L(A;k) = k^{-\beta_L} g_L(A k^{-\nu_L}) \tag{9}$$

was attempted. Figure 3(b) shows an excellent data collapse. The crossover function $g_L(u)$ varies from a power law for small u to a linear relation for large u:

$$g_L(u) = \begin{cases} c_1 u^{\alpha_L} & u \ll u_0 \\ c_2 u & u \gg u_0. \end{cases} \tag{10}$$

The exponent $\alpha_L = 0.5 \pm 0.05$ were determined by a fit for small fractures. The scaling exponents $\nu_L = -1.0 \pm 0.05$ and $\beta_L = 0.55 \pm 0.05$ were determined from the data collapse shown in Fig. 3(b). The behavior is separated by the characteristic area, $\xi_A \propto k^{\nu_L}$, and the corresponding characteristic length, $\xi_L = L(\xi_A)$.

The crossover behavior can again be explained by considering the effect of the substrate attachment. The short explanation is that for small fractures, $L \ll \xi_L$, the fracture is not affected by the substrate attachment and behaves as an elliptical fracture in an unattached spring network, for which the length and the width are proportional and $L \propto A^{1/2}$. For large fractures, $L \gg \xi_L$, the substrate attachment prevents the fracture from widening when it grows at the ends, implying that $L \sim A$. A more precise argument, which also explains the relationships between the scaling exponents, is based on the scaling form of the width $w(x,k)$. The area of the fracture is given by the integral of the width along the fracture:

$$A(L;k) = \int_0^L w(x,k,L)dx. \tag{11}$$

In general the width is also a function of the fracture length, L, $w = w(x,k,L)$. For large fractures ($L \gg \xi_L$) the width has two distinct regimes, a region with a constant, maximum width, and a region close to the tips, where the width varies. The area is the sum of the areas of these regions

$$A(L;k) = 2\int_0^{\xi_w} w(x,k,L)dx + (L - 2\xi_w)w_{\max}. \tag{12}$$

For large L, the main dependence is in the last term, so that

$$L(A;k) = A/w_{\max} = k^{-\beta_L} g_L(Ak^{-\nu_L}). \tag{13}$$

In the limit of large lengths, L is proportional to A. Since $w_{\max} = k^{-\beta_w}$, the scaling relation $\beta_L + \nu_L = -\beta_w$ is obtained from Eq. (13). A similar relation is obtained in the limit of small fractures. Since all the curves $L(A)$ overlap in the unscaled plot in Fig. 3(a) the curve $L(A)$ is independent of k in this region. Assuming that the theoretical behavior, $L(A) = A^{1/2}$, is valid in this limit, we obtain the scaling relation $-\beta_L - \nu_L/2 = 0$. For $\beta_w = 1/2$, the exponents are determined to be $\nu_l = 1$ and $\beta_L = 1/2$, which is very close to the exponents found from the data collapse. The results are therefore consistent with a crossover length ξ_L proportional to the localization length, λ.

The localization effects of the substrate attachment can also be observed in the stress field around the fracture tip. For an elliptic fracture in linear elasticity theory, the σ_{xx} component of the stress tensor decays as a power law $\sigma_{xx} \propto x^{-1/2}$, away from the fracture tip. Figure 4(a) shows a plot of σ_{xx} as a function of distance x from the fracture tip for the single simulated fracture in an ordered material with a substrate attachment spring constant k. For small distances, $x \ll \xi_\sigma$, the stress decays approximately as a power law, $\sigma_{xx} \propto x^{-0.5\pm0.1}$. For large distances, $x \gg \xi_\sigma$, the stress is constant. The crossover length ξ_σ varies systematically with k. The data collapse in Fig. 4(a) indicates that the crossover length is proportional to the localization length λ, since $\xi_\sigma \propto k^{-0.5\pm0.1}$. From the theoretical treatment of an elliptical fracture, the amplitude of the stress component σ_{xx} is known to depend on the fracture length L. The variation of the amplitude is characterized by measuring the stress at a constant distance from the fracture tip, $x = 0$, that is, at the fracture tip for the simulated fracture. Because of the discrete lattice size, the stress does not diverge at the fracture tip in the simulations. The stress at the fracture tip was measured as a function of the number of bonds broken, n, in the fracture, which is proportional to the fracture length L. Figure 4(b) shows a data collapse plot of $\sigma_{xx}(0,n;k)$ for a single simulated fracture. For small lengths, that is, for small values of n, $n \ll \xi_n$, the stress at the fracture tip increases approximately as a power law $\sigma_{xx}(0,n;k) \propto n^{0.4\pm0.1}$. This is very close to the theoretical results for elliptic fractures, for which the amplitude of the stress depends on the square root of the fracture length. For large fractures, $n \gg \xi_n$, the tip stress approaches a constant value. The crossover length ξ_n separating the two behaviors varies systematically with k, and the data collapse again indicates that the crossover length is proportional to the localization length λ.

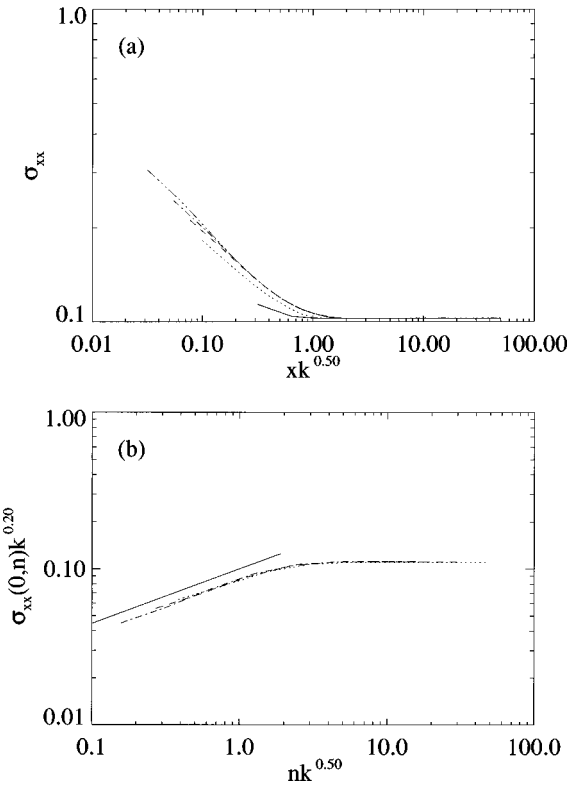

FIG. 4. Part (a) shows the stress component σ_{xx} as a function of distance x from the fracture tip. Part (b) shows a finite-size data collapse plot of the stress component $\sigma_{xx}(0,n;k)$ at the fracture tip ($x = 0$) as a function of the number of broken bonds n.

All the quantities that characterize the fracture shape are therefore related to the localization length λ. For fractures with lengths smaller than λ, or at distances smaller than λ, the fracture is similar to an elliptical fracture described by linear elasticity theory. That is, the substrate attachment does not influence the fracture on these lengths. For fractures significantly longer than λ, the fracture is essentially a line of constant width, which is also proportional to the localization length λ. The behavior of the simulated fracture does, however, deviate from the theoretical description for very small fracture and on very small lengths. We attribute these deviations to the finite lattice size. Very small fracture is not well approximated by an elliptical fracture, because of the finite lattice size.

A similar analysis was applied to study the behavior of the spring-block model. For the spring-block model, the per-

turbation of the stress field away from a broken bond is restricted by the displacement threshold ϵ, which corresponds to a static friction threshold for node displacement. The effect of ϵ on the propagation of the stress field from a single broken bond was first studied in a one-dimensional model. The nodes were initially subjected to a uniform strain t and a bond was removed. The system was relaxed and the total displacement Δx of each node from its initial position was measured as a function of the distance x to the broken bond. The results for $t=1.1$, that is, 10% extension, and varying values of ϵ were consistent with the scaling form

$$\Delta x = \epsilon^{-1.0\pm0.1} g_{\Delta x}(x\epsilon^{1.0\pm0.1}), \tag{14}$$

where the function $g_{\triangle x}(u)$ decays as an exponential function. The decay of a perturbation away from the bond therefore depends on the characteristic length $\lambda_\epsilon \propto \epsilon^{\nu_\epsilon}$, with $\nu_\epsilon = -1.0\pm0.1$. At a distance λ_ϵ away from a broken bond, the strain perturbation is a small fraction of the maximum value. For the one-dimensional system, the behavior is very similar to the behavior for the substrate attachment model.

The quantitative measurements used to characterize the fracture shapes for the substrate attachment model were also applied to the spring-block model. Plots of the width $w(x,\epsilon)$ of the fracture display a behavior similar to the substrate attachment model. At short distances, $x \ll \xi_w$, the fractures behave as elliptical fractures described by linear elasticity theory, and on long distances, $x \gg \xi_w$, the fractures have a maximum width and grow in length only. The characteristic length ξ_w and the maximum width are proportional to the localization length λ_ϵ. Figure 5(a) shows the relation between the fracture length L and the fracture area A for a single fracture in the spring-block model with a displacement threshold ϵ. The curve is consistent with a crossover from a power-law behavior $L \propto A^{0.5}$ for small fractures, $L \ll \xi_L$, to a linear behavior $L \propto A$ for large fractures, $L \gg \xi_L$. The crossover length ξ_L varies systematically with the displacement threshold ϵ. The data collapse in Fig. 5(b) shows that the crossover length ξ_L is a function of ϵ, $\xi_L \propto \epsilon^{0.9\pm0.1}$. The crossover length is therefore proportional to the localization length λ_ϵ for the spring-block model. A direct analysis of the stress field around the fracture tip is also consistent with the picture of a characteristic length ξ_σ, proportional to λ_ϵ, which separates the theoretical behavior of an elliptical fracture from the localized behavior in a large fracture.

The spring-block model behaves similarly to the substrate attachment model. The behavior is separated into two regimes. At small distances and for small fractures, the fracture can be well described as an elliptical fracture in a linearly elastic material. At this scale the fracture is not influenced by the substrate attachment. For large fractures and at large distances the fracture is essentially a line of constant width. The characteristic lengths separating the two regimes are proportional to the localization length λ_ϵ. Some deviations were observed in the data collapses. However, the one-dimensional model indicated that there were deviations in the simple scaling behavior, $\lambda \sim \epsilon^{-1}$, for larger values of ϵ. Due to finite-size effects and restrictions on computer time, the two-dimensional simulations were restricted to larger values of ϵ.

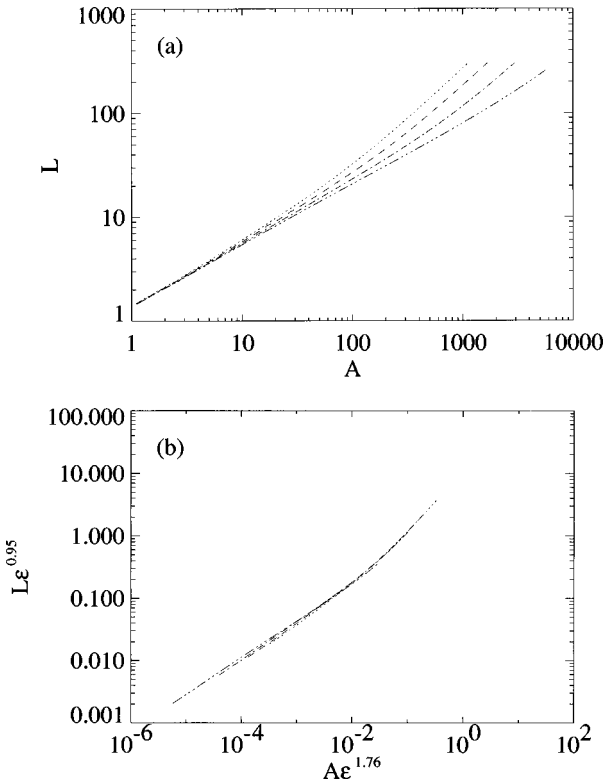

FIG. 5. A plot of the length $L(A;\epsilon)$ as a function of the fracture area A and the displacement limit ϵ for the spring-block model ($\epsilon \gg k$). Part (a) contains a direct plot and part (b) shows a data collapse plot for $\epsilon = 10^{-2}$, 6×10^{-3}, 3×10^{-3}, and 10^{-3}.

Finite-size effects can have a significant influence in these simulations even though they were carried out using periodic boundary conditions on a 400×400 lattice. The stress field from a fracture may propagate around the sample and interact with its images in the infinite periodic lattice generated by the periodic boundary conditions, if the primary lattice is small or the localization length is large. The finite-size effects were examined by varying the system size Λ. For the substrate attachment model, finite-size effects are important for small Λ and k. The form of the function $L(A;k,\Lambda)$ (which describes how the length of the fracture depends on the area A for different values of k and Λ) depends on the lattice size for small lattices as seen in Fig. 6(a). The function crosses over at a length ξ_Λ that increases systematically with Λ. However, for large Λ the function crosses over at a length ξ_k that depends on k. When $\xi_\Lambda > \xi_k$ only the first crossover is observed. The behavior of the model is therefore determined by the smallest of the lengths ξ_Λ and ξ_k. Exactly how ξ_Λ depends on Λ could not be extracted from the data, since the finite-size deviations were small close to the crossover and a large uncertainty was therefore associated with the position of the crossover. For the spring-block model, a similar behavior was observed. The function $L(A;\epsilon,\Lambda)$ crosses over at a length ξ_Λ that increases systematically with Λ as seen in Fig. 6(b). However, for the given value of ϵ the region in which ξ_Λ exceeded ξ_ϵ was not reached, since only a limited range of Λ values were available due to restrictions on computer time. The computer time needed for a simulation increases rapidly with both Λ and ξ_ϵ. Again, the exact dependence of ξ_Λ on Λ could not be determined. These

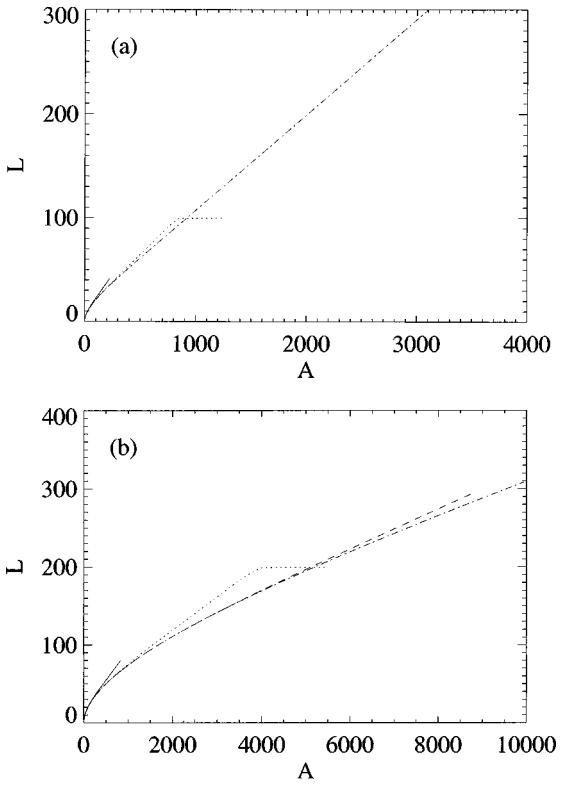

FIG. 6. Finite-size scaling plots for the length L as a function of A for a singe fracture. Part (a) shows $L(A;k=10^{-3},\Lambda)$ for the substrate attachment model and part (b) shows $L(A;\epsilon=6\times10^{-4},\Lambda)$ for the spring block model. The curves are for $\Lambda=50,100,200,400$. The deviations are systematic in Λ.

finite-size effects restricted the parameter range that could be tested by the simulations. For smaller values of k and ϵ, larger lattices were needed to avoid finite-size effects, and, in addition, the simulation time for identically sized lattices increased. The range of values available for k and ϵ were therefore limited.

IV. MANY FRACTURES IN A DISORDERED MATERIAL

The computer model can be used to simulate the fracturing of a material layer attached to a deformable substrate. In general, such systems do not consist of a single fracture, but many, interacting fractures that nucleate, grow, and merge. The stress at a particular point in the material depends on all the fractures in the sample, within the localization length determined by the substrate attachment. Since both growth and nucleation of fractures depend on the local stress, it is not sufficient to study a single fracture. The whole system must be considered to address the behavior of the fracture pattern. To model disordered materials such as rock and clay, the local variation of material properties must be included. The material is assumed to be homogeneous on scales much larger than the length of a single spring, which is realistic for clay, since clay, unlike rock, is homogeneous on long length scales. On smaller scales the material is disordered. The material properties of the springs are drawn from random distributions to simulate the quenched disorder, which is frozen into the spring network. Here, the equilibrium length and spring constant were constants, and only stress thresholds for each spring were selected randomly. The material behavior is determined by the randomly distributed stress thresholds. Several families of distributions were tested. The results most similar to clay were obtained with a Gaussian distribution with average μ and standard deviation σ. The behavior of the network varied with μ and σ. A very narrow distribution resulted in a brittle material: A single straight fracture propagated across the sample. For a wider distribution the material behavior was more ductile.

The model is not restricted to simulate materials that are homogeneous on large scales. Specific inhomogeneities can be included in the model by changing the material properties in particular regions of space. The model produces a wide range of patterns for different distributions of breaking thresholds. Centralized distributions, such as a uniform distribution or a Gaussian distribution produce similar patterns, and are represented here by a Gaussian distribution of thresholds. However, other types of distributions have also been tested. For example, exponential distributions, for which most bond strengths were small, produced very dilute patterns. These patterns were not similar to naturally occurring patterns, such as in clay, since most bonds fractured randomly at small strains, when the stress field was not important for the fracture development.

Fracture patterns from simulations in the substrate attachment model and the spring-block model are shown in Fig. 7 and Fig. 8, respectively. All the simulations are for the same material properties, a Gaussian distribution of breaking thresholds was used with $\mu=1.15$ and $\sigma=0.05$, but the substrate attachment constants k and ϵ were varied. The patterns in the two models have many common features. For example, both patterns are characterized by an average spacing between the fractures, and by the correlations between the fractures: Long fractures are tailed by smaller fractures close to the fracture tips and fractures tend to form bands of almost connected fractures. In the following, we characterize the fracture patterns statistically and visually. The statistical properties of individual fractures, such as their self-affine scaling properties, are studied, and statistical measures are applied to describe the dynamics of the fracturing process.

A striking feature of the patterns in both the substrate attachment model and the spring block model is the approximate uniform spacing of the fractures. The spacing appears to vary systematically with the attachment parameters k and ϵ. Studies of a single fracture in an ordered material (see Sec. III) show that the substrate attachment introduces a characteristic length scale, the localization length λ, that determines the stress decay around the fracture and the shape of the fracture. A similar characteristic length is expected to be reflected in the fracture patterns for a disordered material. A fracture releases strain in the regions surrounding the fracture. In the direction normal to the direction of fracture propagation, the stress increases with the distance from the fracture, and approaches a constant value far away from the fracture. In one dimension, the stress increment can be found exactly. The substrate attachment induces an exponential localization of the relaxation close to the fracture, characterized by the localization length λ. This is the case for both the substrate attachment model and the spring-block model, however, for the spring-block model the one-dimensional results are not known exactly, but were determined from the

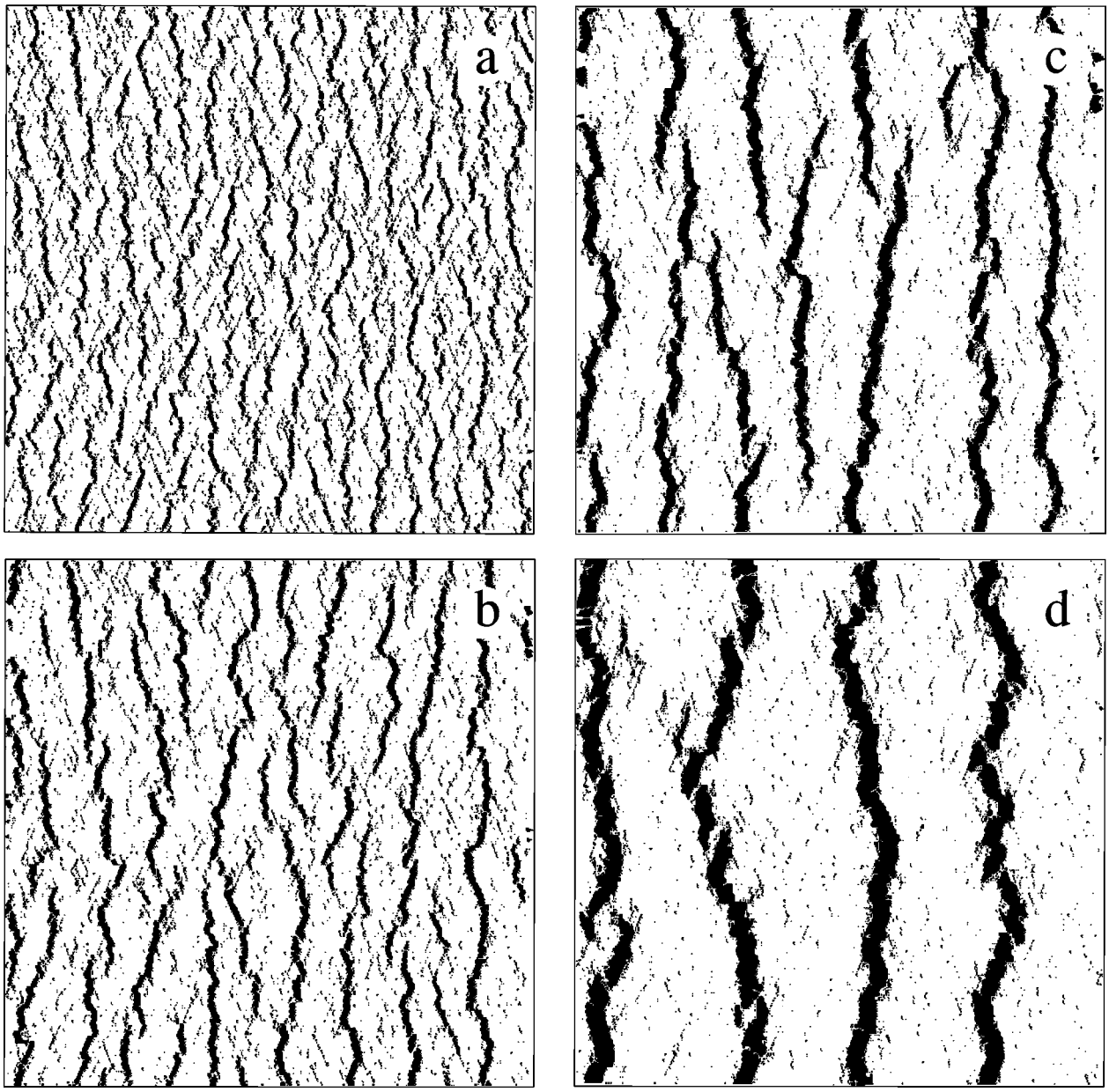

FIG. 7. Picture of the fracture patterns from simulations using a 200×200 substrate attachment model with $\epsilon=k/300$ and a Gaussian distribution of breaking thresholds with $\mu=1.15$ and $\sigma=0.05$. The pictures are for 20% extension of the substrate for $k=0.03,0.01,0.003$ and 0.001 from top left to bottom right.

simulations. This stress increment controls the nucleation and growth of nearby fractures. A similar effect is expected in two dimensions. And, indeed, in the case of a single fracture in an ordered material, a decay of the perturbations characterized by a characteristic length λ was observed. Beyond a distance λ, the perturbation from an open fracture, for example the relaxation from an open fracture, is negligible. Because of this effect, the spatial distribution of fractures is correlated, and the appearance of a characteristic distance between the fractures in the direction of the externally imposed strain is expected. The spacing in the simulated patterns was characterized by measuring the average distance between fractures, Δl. Figure 9 shows plots of the average spacing as a function of k and ϵ for the substrate attachment model and the spring-block model, respectively. The curves are consistent with power laws. For the substrate attachment model, $\Delta l\propto k^{\nu_k}$, with $\nu_k=-0.4\pm0.1$. The average spacing is, therefore, within the uncertainties, proportional to the localization length λ. Similarly, for the spring-block model, $\Delta l\propto\epsilon^{\nu_\epsilon}\propto\lambda_\epsilon$, with $\nu_\epsilon=-1.1\pm0.1$. Consequently, the average spacing is proportional to the localization length for both models.

Several statistical measures were applied to characterize the simulated fracture patterns. The size distribution of fractures is frequently used to characterize fracture patterns. Figure 10 shows plots of the probability density $P(L)$ for a fracture of length L. [The probability for a fracture to have a length in the interval L to $L+dL$ is $P(L)dL$.] The different distributions correspond to the patterns shown in Fig. 7 and Fig. 8. For the spring-block model [Figs. 10(a) and Fig. 8], the distribution crosses over for small and large fractures. Crossovers are also expected for small and large fractures. In

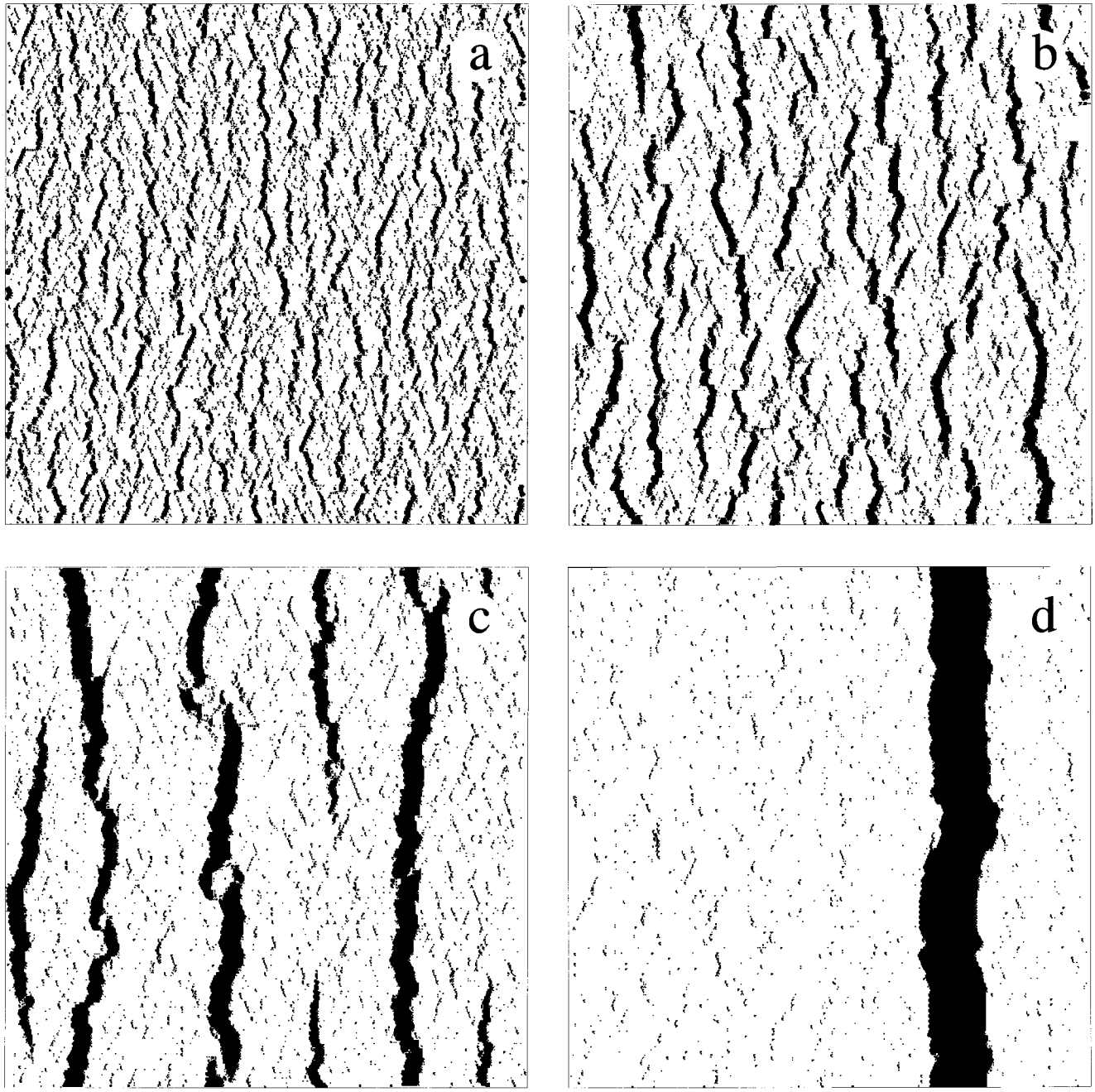

FIG. 8. Picture of the fracture patterns from simulations of a 200×200 spring-block model with a Gaussian distribution of breaking thresholds with $\mu=1.15$ and $\sigma=0.05$. The pictures are for 20% extension of the substrate for $\epsilon=0.002$, 0.001, 0.0005, and 0.0001 from top left to bottom right.

the simulated patterns, there are many small fractures that result from the random breaking of a single or just a few bonds. The number of these fractures depends on the distribution of breaking thresholds and the density of very weak bonds, and are not a result of the interaction between fractures and the stress field that characterize larger fractures. Very small fractures, with a length smaller than a few lattice constants, should therefore be ignored. Large fractures are restricted by the localization length, which is reflected in the cutoff in the probability density $P(L)$ for large fractures. In the intermediate range, between these two crossovers, the characteristic behavior of the model can be observed. In this region, the behavior might be consistent with a power law, however, the scaling region is too narrow to distinguish the behavior from a crossover between two non-power-law regimes.

The probability density of fracture lengths for the substrate attachment model is shown in Fig. 10(b). The different distributions correspond to the patterns shown in Fig. 7. The size distribution is similar to the distribution observed for the spring-block model. The distribution varies systematically with k, however, there is no clear power law region in the distribution. The data therefore suggest that there is no general power-law form for the size distribution of fractures in these models.

The measurement of the fracture length L as a function of

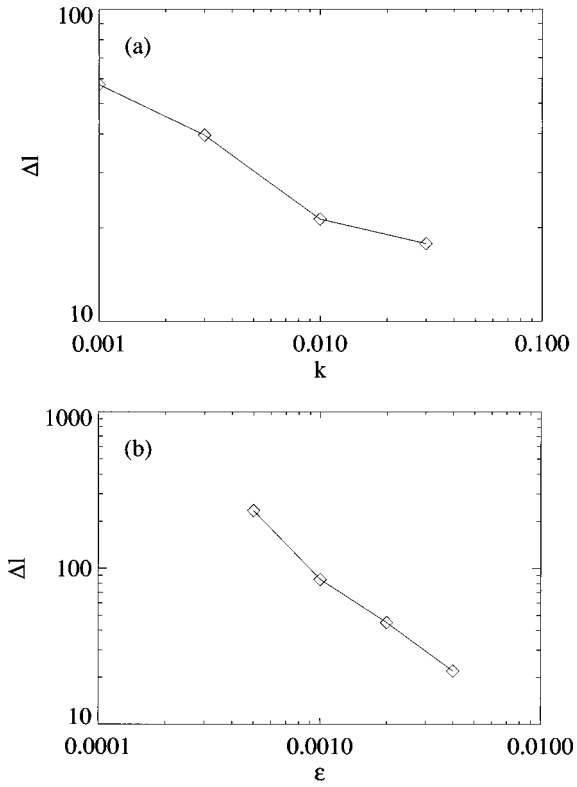

FIG. 9. Plots of the average distance between fractures, Δl, as a function of the substrate attachment constant, k [part (a)] or the movement threshold ϵ for the spring-block model [part (b)]. The simulations are for a 200×200 system with a Gaussian distribution of thresholds ($\mu=1.15$, $\sigma=0.05$).

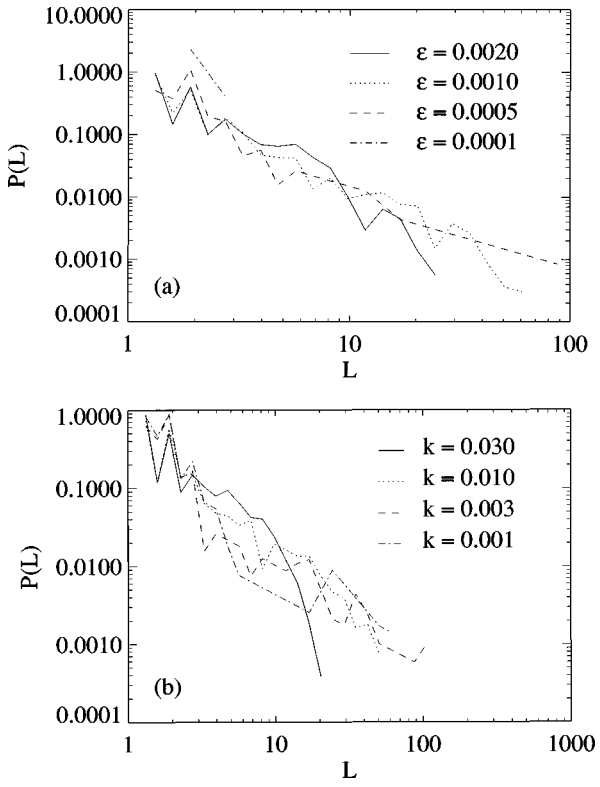

FIG. 10. Plot of the probability density $P(L)$ as a function of the fracture length L for simulations on a 200×200 lattice with a Gaussian distribution of breaking thresholds with $\mu=1.15$ and $\sigma=0.05$. Part (a) is for the spring block model with $\epsilon=0.002$, 0.001, 0.0005, and 0.0001. Part (b) is for the substrate attachment model with $\epsilon=k/300$. The curves are for different values of the substrate attachment spring constant, $k=0.001$, 0.003, 0.01, and 0.03.

the open fracture area A was recently proposed to characterize patterns of interacting fractures. Since the simulated fractures are, to a good approximation, oriented perpendicular to the direction of extension, a fundamental measurement of their length is the length in this direction. For simulations of the spring block model, plots of $L(A)$ are shown in Fig. 11(a) for different values of ϵ. Several crossover regimes are expected for this model. For small fractures, $A<5$, the fracture length is proportional to the fracture area A. In this limit, the finite lattice size is important: Fractures grow in length without growing significantly (compared with the lattice size) in width. For large fractures, another crossover to a linear behavior is expected. Due to the localization length, the fractures have a maximum width. The crossover length at which the upper crossover occurs, depends on the friction threshold ϵ as is evident from Fig. 11(a). A possible power-law region of the relation $L(A)$ must be extracted from the intermediate scale between the two crossover regions, but the region between the two crossovers is too small to assess the behavior, even for the smallest values of ϵ used in the simulations. A very similar behavior was observed for the substrate attachment model. Figure 11(b) shows the curves $L(A)$ for different values of k. Again, two crossover regions are observed and the intermediate region is too narrow to distinguish a power-law behavior from the crossover regions.

For the simulations on the 200×200 lattice, the dynamic range of fracture sizes was too small to determine the scaling behavior for both the size distribution and the relation between length and area. A larger span between small fractures and the characteristic length scales given by the localization lengths are needed. However, the computation time increases rapidly with system size and with decreasing values of both k and ϵ. It was therefore difficult to carry out large simulations with large localization lengths. In order to study large systems, a modified version of the spring-block model was introduced, in which all nodes were displaced initially during relaxation, irrespective of the displacement threshold. This model behaved similar to the spring-block model, but the amplitude $\mathcal{A}$ of the localization length scaling relation, $\lambda=\mathcal{A}\epsilon^{-1}$, was increased. A larger value of ϵ could therefore be used and larger systems could be simulated. We term this model the hybrid model and use it to study large scale fracture patterns. Figure 12 shows pictures from simulations for different system sizes ranging from $\Lambda=100$ to 800. These simulations are analyzed using the statistical measures introduced above.

The size distribution of fractures is shown in Fig. 13. For both the probability density of fractures, $P(L)$, and its integral, the cumulative distribution is shown for different system sizes. The distribution again displays two crossovers. The small fracture region is dominated by many small, random fractures as discussed above. For large fractures, the finite system size Λ introduces a cutoff in the size distribution. The plot in Fig. 13 indicates that the cutoff length increases systematically with the system size Λ. From the cumulative distribution, the behavior in the intermediate region

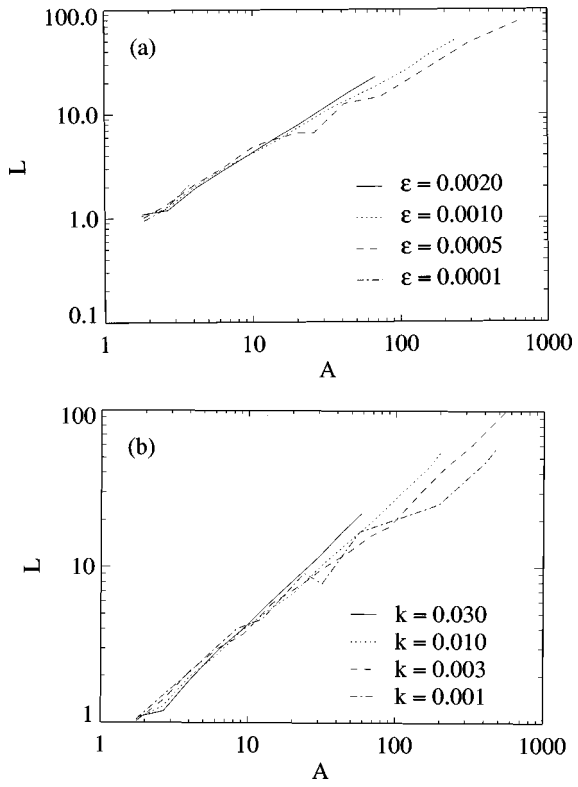

FIG. 11. Plots of fracture length L as a function of open area A for simulations on a 200×200 lattice with a Gaussian distribution of thresholds ($\mu=1.15$, $\sigma=0.05$). Part (a) is for the spring-block model with $\epsilon=0.002$, 0.001, 0.0005, and 0.0001. Part (b) is for the substrate attachment model with $\epsilon=k/300$ and $k=0.03$, 0.01, 0.003, and 0.001.

appears to be described by a power law with an exponent of -0.3 ± 0.1, which corresponds to a power law with exponent -1.3 ± 0.1 for the probability density, and the scaling region increases with system size. However, the plot of the probability density shows that the effective exponent clearly depends on the system size. A power-law interpretation is therefore not supported by the data.

The relation between the fracture length L and area A are shown in Fig. 14 for different system sizes. Due to the finite lattice size, the fracture length is proportional to the area for small fractures. For large fractures, a power-law relation $L\propto A^{\beta}$ is observed, where $\beta=0.72\pm0.03$. Simulations for varying system sizes indicate that there is a crossover for large fractures, but that the range of the scaling region increases systematically with system size. No effect of a localization length was observed in this case.

Not only the fracture patterns, but also the individual fractures in the patterns, have statistically varying properties. From Fig. 12 it can be seen that a single fracture is not only characterized by the width along the fracture, but also by its deviations from a straight line. The deviations can be characterized by the width of the deviation, Δx, in the x direction for a fracture of length Δy in the y direction. If the fractures behave as random walks in the x direction, the relation $\Delta x\propto\Delta y^{1/2}$ is expected. A generalization is a self-affine fractal with a roughness (Hurst) exponent H, for which the relation $\Delta x\sim\Delta y^{H}$ is expected. Figure 15 shows plots of Δy as functions of Δx for the spring-block model. Since the width of the fracture varied along its length, Δx was measured as the deviation of the center line or the edge of the fracture. For large simulations of the spring-block model, the relation $\Delta y(\Delta x)$ is consistent with a power law with exponent 2.0 ± 0.1, indicating a self-affine scaling with a Hurst exponent $H=0.5\pm0.1$. For small fractures, a crossover due to the finite lattice size is observed. For large fractures, a crossover that depends systematically on the system size Λ is observed, indicating that the finite system size produces the upper crossover. In an intermediate range, a power-law behavior $\Delta x\propto\Delta y^{H}$, with a Hurst exponent $H=0.5\pm0.2$, is observed.

The measurement of the deviations and the lengths of all fractures in the pattern characterize the ensemble of fractures. The deviations of each fracture can also be characterized individually by the two-point correlation function. For a fracture along the y direction with an edge (or center–line) given as $x(y)$, the point-point correlation function is

$$C_2(y)=\langle[x(y_0+y)-x(y_0)]^2\rangle_{y_0}. \tag{15}$$

For a self-affine fractal curve $x(y)$, the correlation function has the form

$$C_2(y)\propto y^{2H}. \tag{16}$$

A plot of the correlation function averaged over the 5 largest fractures is shown in Fig. 15 for the large-scale simulations. Over a limited range, the correlation function is consistent with a power-law with exponent 1.0 ± 0.2, which indicates a Hurst exponent $H=0.5\pm0.1$. However, the fractures are small and the dynamic range (the difference between the largest and smallest length) is therefore too small for this method to provide reliable results.

The dynamics of the development of the fracture pattern contains many interesting features that can be studied in the simulations. Since the development of the spring-block model and the substrate attachment model did not differ significantly, only the dynamics of the spring-block model is discussed. A simple illustration of the dynamics is given by a plot of the number of broken bonds, N, as a function of the imposed extension t as shown in Fig. 16. The development of the pattern is described by the following sequence of events: For small extensions most of the deformation is taken up as strain in the springs. Small fractures appear as a result of randomly placed low breaking thresholds. This behavior is termed the random nucleation regime. When the imposed extension increases and the strain in the springs approaches the average breaking threshold, the stress intensification at the fracture tips becomes large enough to propagate the fractures and induce avalanches of rupture events. This avalanche regime is observed as the steep portion of the curve in Fig. 16. At even further extension most of the deformation is taken up by a widening of the already existing large fractures and most ruptures occur at the fracture tips. For the substrate attachment model, a sequence of avalanche regimes followed by fracture widening and growth appear as extension is increased. However, most simulations were stopped during the first widening regime. Simulations were performed for different system sizes Λ. The number of broken bonds at 20% extension, $N(0.20)$, is not proportional to Λ^2 as naively ex-

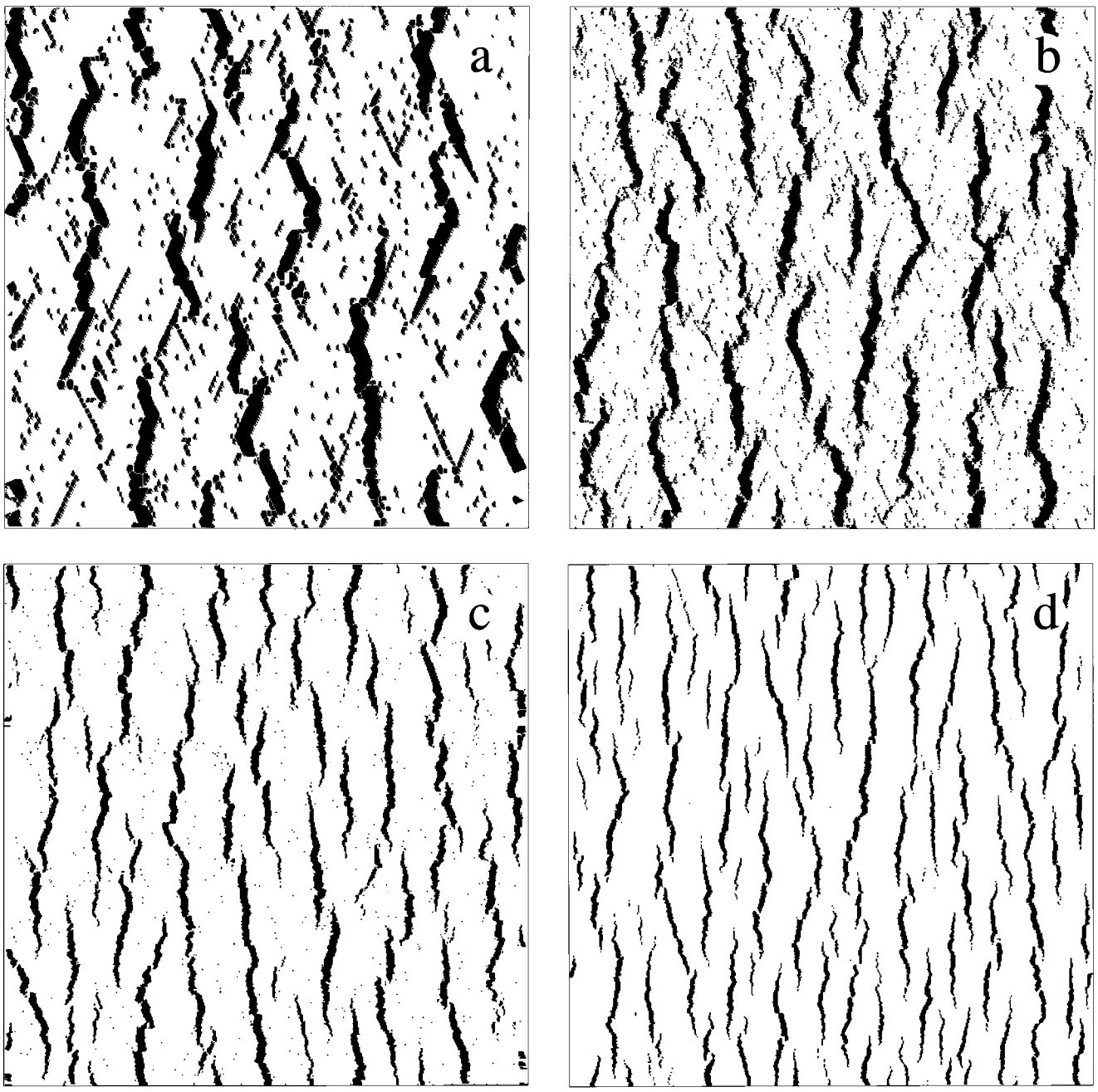

FIG. 12. Picture of the fracture patterns from simulations with $k=0$ and $\epsilon=0.008$ for different system sizes Λ. The pictures are for 20% extension for $\Lambda=100$, 200, 400, and 800 from the top left to bottom right.

pected, but $N(0.20)\propto\Lambda^{1.66\pm0.1}$. For larger systems more of the externally imposed deformation must therefore be taken up by fracture widening.

The number of broken bonds is a model-specific quantity. A more physical quantity is the total open area of fractures, $A(t)$. This quantity can also be measured experimentally. A plot of the development of A for the spring-block model is shown in Fig. 17. For small extensions, the total open area is small and approximately constant. For larger extensions the behavior crosses over to a linear dependence on the extension.

V. DISCUSSION

The numerical model is intended to simulate the fracturing in a material with a large length to depth ratio attached to a deformable substrate. The real test of the model is to what degree it reproduces the fracturing observed in experimental studies. A direct comparison between simulation and experiment depends on reliable statistical measures of the fracture pattern, the properties of single fractures and the dynamics of the fracturing process. Here, we compare the fracture patterns from simulations with patterns from experiments using the quantitative measures presented previously.

Figure 18 shows the fracture pattern from a hybrid model simulation and the fracture pattern from an extensionally deformed clay slab [13]. In the experiment a clay cake was placed on the concave side of a bent metal plate that was slowly restored to a flat position, inducing a uniform extension of 20% at the top surface of the clay cake as described by Walmann *et al.* [13]. The fractures were visualized by

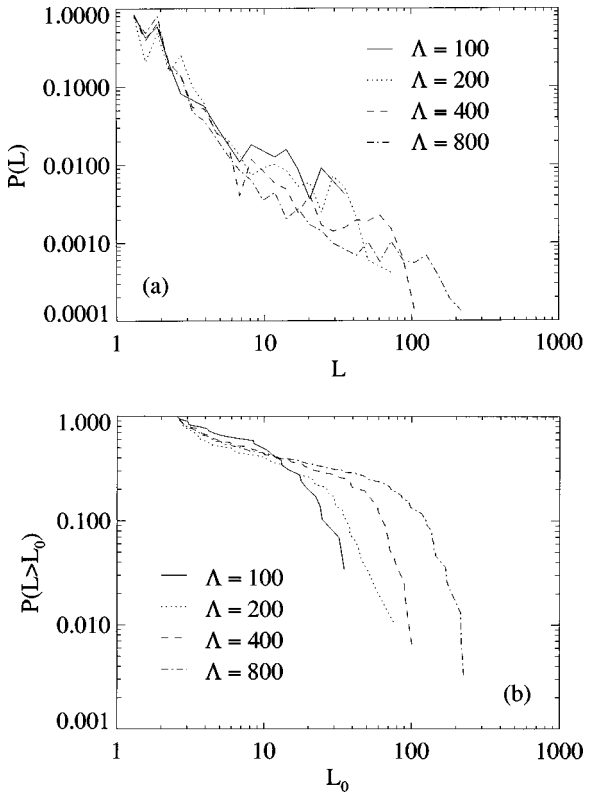

FIG. 13. The distribution of fracture length L for simulations for $\epsilon=0.008$ with a Gaussian distribution of breaking thresholds with $\mu=1.15$. Part (a) shows the probability density $P(L)$ and part (b) shows the cumulative distribution $P(L>L_0)$. The probability density has been logarithmically binned. The curves are for different system sizes $\Lambda=100$, 200, 400, and 800.

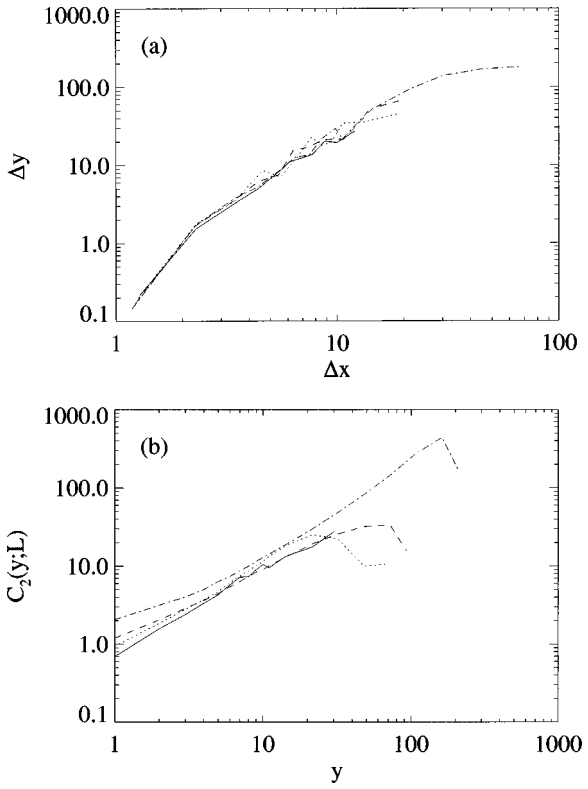

FIG. 15. Part (a) shows plots of the deviation, Δx, as a function of fracture length, Δy, for a spring-block model with $\epsilon=0.008$. The different curves are for system sizes $\Lambda=100$, 200, 400, and 800. Part (b) shows plots of the correlations function, $C_2(y;\Lambda)$, for the 5 largest fractures in the spring-block model for $\epsilon=0.008$. The different curves are for differing system sizes $\Lambda=100$, 200, 400, and 800.

coloring the initial clay surface with a fine, black powder. The open fractures were gray, which gave a good contrast to the black, powdered clay. In the picture, the open fractures are shown as black regions. Visually, the correspondence between the fracture pattern from the hybrid model and the experimental fracture pattern is very good. The simulation model reproduces many of the important features of the clay fracture patterns. For example, fractures tend to line up in bands and small fractures frequently start close to the ends of large fractures. A striking feature of the experimental fracture pattern is the approximately uniform spacing of fractures. For the simulation model, the average spacing is controlled by the localization length, determined by the parameters k or ϵ. The average spacing in the model can be tuned to the value observed in the clay. The average spacing observed in the clay experiments also indicates that a length scale corresponding to the localization length is present in

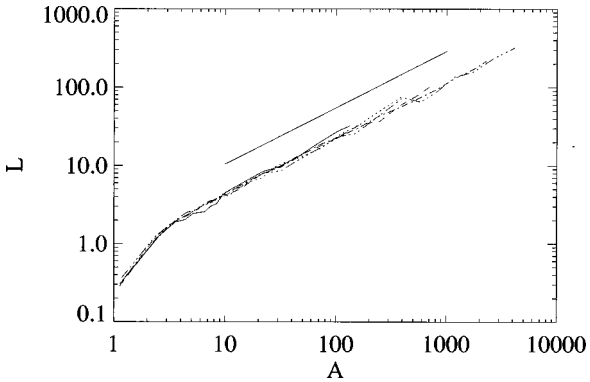

FIG. 14. Plots of fracture length L as a function of open area A for simulations with a Gaussian distribution of thresholds ($\mu=1.15$, $\sigma=0.05$) for $\epsilon=0.008$. The curves are for different system sizes $\Lambda=100$, 200, 400, and 800. The drawn line shows a power law $L\propto A^{\beta}$, with $\beta=0.7$.

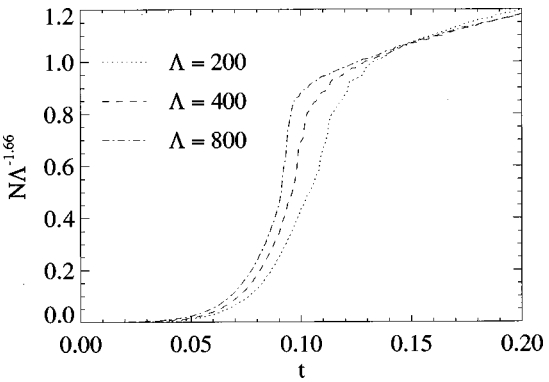

FIG. 16. A plot of the cumulative number of bonds N broken as a function of substrate extension t in the spring-block model with $\epsilon=0.008$. The extension was increased in steps of $\delta t=10^{-3}$. The curves are for system sizes $\Lambda=200$, 400, and 800. The plot is scaled with the system size Λ.

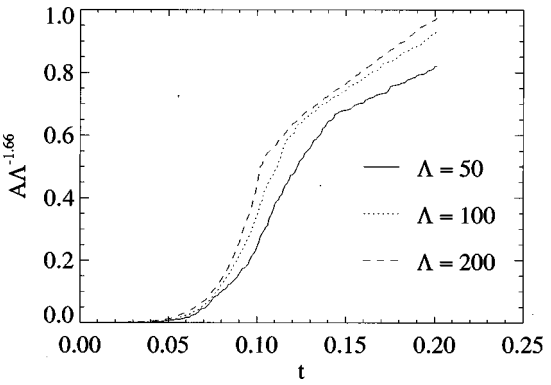

FIG. 17. A plot of the total open fracture area A as a function of the substrate extension t for the spring-block model on a 400 $\times$400 lattice. There are deviations from a universal behavior for small systems. The plot is scaled with the system size Λ.

the clay sample, and we assume that the length scale is related to the height of the clay cake. There is considerable experimental evidence that relates the height of a deformed layer to the average fracture spacing [30,31]. An average spacing is characteristic of thin layers attached to deformable substrates, and indicates that a simulation model with a substrate attachment is a reasonable approximation.

Statistically, the experimental fracture pattern has been characterized by the fracture size distribution and the relation between fracture length and area. For the experimental system, the size distribution was not consistent with a power law, and no other simple functional form was found to describe the distribution. A direct comparison with the simulated patterns is therefore difficult. However, the general form of the distribution is qualitatively similar to the distribution observed for the simulations.

For the experimental fracture pattern, a very robust scaling relation between the fracture length L and open area A was observed, $L \propto A^{\beta}$, where $\beta = 0.67 \pm 0.02$. Deviations due to the finite image resolution were observed for small fractures, for which a direct proportionality was found. However, for large fractures the scaling relation was insensitive to changes in deformation type and rate, within certain limits [13]. A similar behavior was observed in the simulation models, but crossovers were observed for both small and large fractures. For small fractures a crossover to a linear behavior was expected, due to the finite lattice size. For the substrate attachment model and the spring-block model, crossovers were observed for large fractures due to localization effects at lengths larger than the localization length. However, the localization length could not be increased sufficiently to provide a large enough dynamic range between the two crossovers to establish a power-law relation because the computation time increased rapidly with localization length. For the hybrid model, on the other hand, the upper crossover increased systematically with system size. In an intermediate range between the two crossover lengths, the relation $L(A)$ was consistent with a power-law behavior $L \propto A^{\beta}$, with $\beta = 0.72 \pm 0.03$, which is very close to the experimentally observed relation. However, we should be particularly careful in this case, since no separate crossover dependent on the localization length was observed for the hybrid model. For the hybrid model the localization length depends

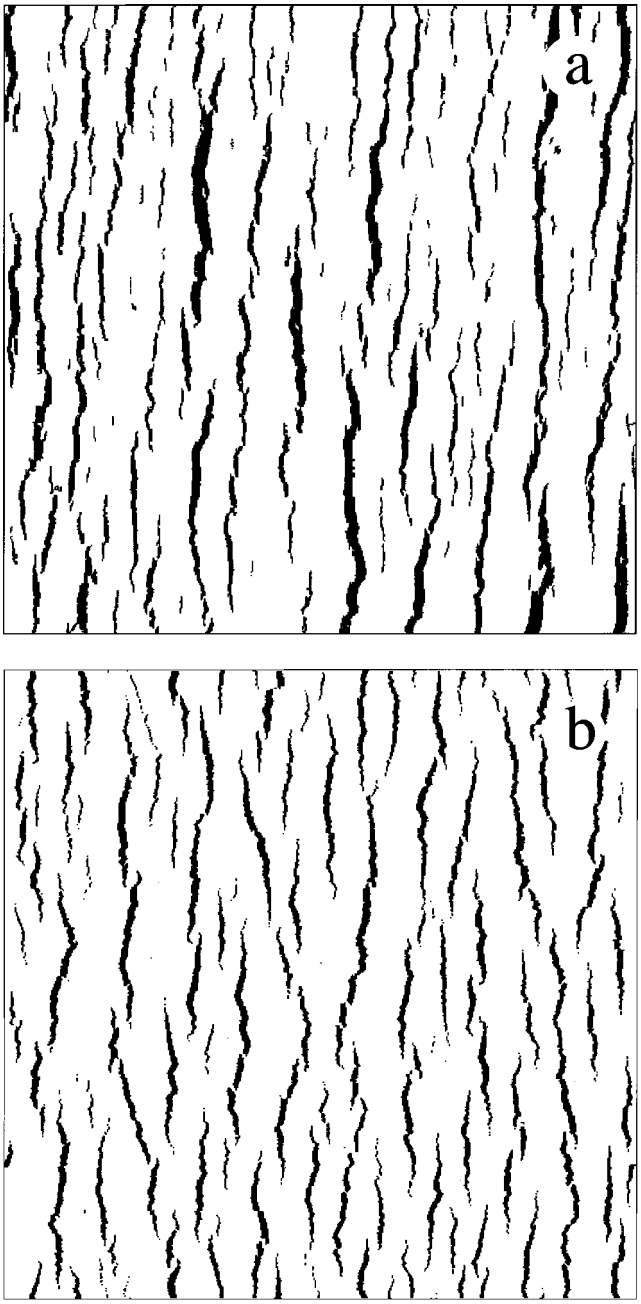

FIG. 18. A picture from an experiment of clay in [13] are shown in part (a) and part (b) shows a picture from a simulation of a 800$\times$800 lattice with $\epsilon = 0.008$ and $k = 0$ for a normal distribution of thresholds ($\mu = 1.15, \sigma = 0.05$). Both pictures correspond to 15% extension.

on the system size since all nodes are moved in the first relaxation step irrespective of the forces acting on them. The propagation of a perturbation in the stress field therefore depends on the number of relaxation cycles initiated, which depends on the number of bonds broken that in turn depends on the system size. Consequently, the crossover length associated with the localization is also expected to scale with system size. Two upper crossover lengths are expected in the plot of $L(A)$, one length that depends on the finite system size and one length that depends on the localization. The observed crossover length is the lowest of the two. The behavior of $L(A)$ is therefore consistent with a power-law re-

lation $L \propto A^{\beta}$ in an intermediate range, but we cannot rule out the possibility that the observed behavior is the result of the interplay between two crossover regions appearing at different lengths. The conclusion would be more convincing if a similar behavior could be found in the substrate attachment model or the spring-block model by varying only a single length scale, the localization length. Unfortunately, we cannot perform simulations with large enough localization lengths due to computer time limitations.

The effect of the localization length was also observed for the simulation of a single fracture in an ordered material, for which the relation between length and area crossed over from a power-law relation to a linear relation at a crossover length that was proportional to the localization length. However, for a single fracture the relation $L(A)$ characterizes different features of the fracturing process than for the case of interacting fractures in a disordered material. For the single fracture, the relation describes the development of a fracture that does not interact with other fractures, whereas for the disordered system, the relation describes the statistics of the fracture pattern and the relation between large and small fractures at a given time in the development of the pattern.

The presented measurements of fracture roughness are uncertain because of the limited range of deviations and fracture lengths. The fractures could not be distinguished from random walks, but the scaling behavior is not conclusive. There are also no relevant experimental data for comparison, because of similar resolution problems for experiments. However, for experiments on uniform extension in powder [32], the fractures were found to be self-affine fractals with a Hurst exponent of approximately $H = 0.7 \pm 0.05$. This is significantly higher than the value found here for the simulation model, although the relevance of this exponent is not clear.

The dynamical development of the fracture pattern in model and experiment is also very similar. The only quantitative measure available in the experiments is the fractured area as a function of extension, $A(t)$. In the experiments, $A(t)$ has a small, approximately constant, value for small extensions. For intermediate extensions the total fractured area increases rapidly with extension and for large extensions a linear relation $A(t) \propto t$ is observed [13]. A similar behavior was observed in the simulations, for which the transitional regime was more pronounced.

VI. CONCLUSIONS

Two related models for fracturing in layers of material attached to deformable substrates have been studied. In the substrate attachment model, the simulated layer is attached to a deformable substrate with springs, and in the spring-block model the layer is placed on the deformable substrate and sticks due to static friction forces. The models are similar in that they both have a characteristic length scale associated with the substrate attachment that restricts the propagation of the stress field. For single fractures in an ordered material the models are consistent with linear elasticity theory on short length scales, however, the propagation of the stress field is cut off at large length scales. The dependence of the localization length scale, λ, on the system parameters differs for the two models. For the substrate attachment model $\lambda \propto k^{-1/2}$, where k is the substrate attachment spring strength. For the spring-block model $\lambda_{\epsilon} \propto \epsilon^{-0.9 \pm 0.1}$, where ϵ is the static friction threshold between blocks and substrate. In addition, a hybrid model was introduced in order to simulate large systems of disordered materials. The hybrid model is similar to the spring model, but the localization length is a function of both ϵ and system size and increases with system size.

The original motivation for studying modifications of the substrate attachment model was to understand the importance of the relaxation parameter, ϵ. This study shows that the behavior is dominated by the substrate attachment when the localization length from the spring-block behavior, λ_{ϵ}, is larger than the localization length for the substrate attachment springs λ_k. However, both the substrate attachment and spring-block models have interest in themselves, and both models represent reasonable representations of the coupling between the simulated material and the supporting substrate. For all models, the behavior is characterized by a localization length. The dependence on material properties and deformation history is also similar for all models, and the patterns produced by the different versions of the model are visually and statistically similar. Many of the features of the models, such as their dynamic development, are also common. It is therefore reasonable to discuss and refer to the models as one common model, the substrate supported spring model, characterized by a localization length. However, there are also differences between the model modifications that can be important. For example, in the spring-block model a node loses memory of its original position after it has been moved, whereas in the substrate attachment model a node is always connected to its original substrate position. These features might be important for larger systems, at larger deformations or for different material properties than what we have used here.

The models were used to simulate fracture patterns in disordered materials for comparison with clay. Here we have concentrated on Gaussian distributions of breaking thresholds, which produced results similar to those found in laboratory clay model experiments. Statistical comparison between model and experiment was based on the size distribution of fractures and a relation between fracture length and area. The size distribution of fractures is of interest and importance in itself and has frequently been used to characterize fracture patterns. A variety of studies [33–35] have suggested that in many geological systems the size distribution is a power law. Neither experiments nor any of the simulation models displayed a convincing power-law behavior and no other appropriate functional form was found. Even though the behavior of the size distribution was qualitatively similar to experimental results, a direct quantitative comparison was not possible.

A more quantitative comparison between experiments and models was achieved using a recently proposed scaling relation between the length and the width of fractures in a fracture pattern. The fracture length varied consistently as $L \propto A^{\beta}$ for large fractures in the experiments and over a range limited by the localization length in the simulations. However, for the substrate attachment and spring-block models, the behavior could not be distinguished from crossover between non-power-law regions because the dynamic range

was too small, whereas an intermediate power-law behavior was established for the hybrid model. The exponent $\beta = 0.72 \pm 0.03$ found in simulations with the hybrid model was also within the uncertainties of the experimental value $\beta = 0.68 \pm 0.02$. We cannot, however, discard the possibility that the scaling observed in the hybrid model is an *effective* scaling resulting from the overlap of several crossover regimes. Nevertheless, the data do not indicate that there is more than one upper crossover length, and the observed crossover length increases systematically with the system size (and the localization length), which indicates a power-law behavior in the limit of large localization lengths. The scaling relation, $L \propto A^{\beta}$, is a very robust measure, which is valid for several different extensional deformations, including graben deformations. The relation is therefore suitable for comparisons between models and experiments and can be an important characterization of patterns of interacting fractures. For the growth of a single fracture, the fracture width is proportional to the fracture length and the relation $L \propto A^{1/2}$ was observed. A similar experimental study is not available for comparison, but this is consistent with results from geological field studies (see, for example, [36]).

The substrate supported simulation model reproduces the most important visual and statistical properties and the dynamical development of the clay fracture pattern. We find the good correspondence encouraging since the model is strictly two dimensional and fractures and faulting in a clay slab is a three-dimensional process. The model produces many of the correlations between fractures obvious from pictures of clay experiments. This indicates that some of the important aspects of the clay experiments can be understood without resorting to three-dimensional models. The experimental fracturing patterns are difficult to reproduce using purely statistical modeling approaches. Consequently, relatively simple two-dimensional models, like those described in this paper, may find important applications in the modeling of oil reservoirs and pollution transport. This study was limited to extensional fractures in clay materials, since quantitative experimental results were available only for this scenario. The model should, however, also be applicable to other deformations, but new features might be needed to simulate shear and compression. This is subject for further study and will be addressed later.

ACKNOWLEDGMENTS

This work was supported by VISTA, a research corporation between the Norwegian Academy of Science and Letters and Den Norske Stats Oljeselskap (STATOIL), and has received financial support and a grant of computing time from the Norwegian Research Council.

[1] B. B. Mandelbrot, D. E. Passoja, and A. J. Paullay, Nature (London) **308**, 721 (1984).
[2] R. H. Dauskardt, F. Haubensak, and R. O. Ritchie, Acta Metall. Mater. **38**, 143 (1990).
[3] B. L. Cox and J. S. Y. Wang, Fractals **1**, 87 (1993).
[4] P. Meakin, Phys. Rep. **235**, 189 (1993).
[5] K. J. Måløy, A. Hansen, E. L. Hinrichsen, and S. Roux, Phys. Rev. Lett. **68**, 213 (1992).
[6] E. Bouchaud, G. Lapasset, and J. Planès, Europhys. Lett. **13**, 73 (1990).
[7] J. Hall, Philos. Trans. R. Soc. London **7**, 79 (1815).
[8] *The Deformation of the Earth's Crust*, 2nd ed., edited by W. H. Bucher (Princton Univeristy Press, Princeton, NJ, 1941).
[9] H. Cloos, Centralbl. Mineral. Pal. **5**, 609 (1928).
[10] H. Cloos, Naturwissenschaften **34**, 741 (1930).
[11] Oertel, Tectonophysics **2**, 343 (1965).
[12] V. V. Belousov and M. V. Gzovsky, in *Physics and Chemistry of the Earth*, edited by L. H. Ahrens, F. Press, S. K. Runcorn, and H. C. Urey (Pergamon Press, Oxford, 1965), pp. 409–499.
[13] T. Walmann, A. Malthe-Sørenssen, J. Feder, T. Jøssang, P. Meakin, and H. H. Hardy, Phys. Rev. Lett. **77**, 5393 (1996).
[14] S. J. Zhou, P. S. Lomdahl, R. Thomson, and B. L. Holian, Phys. Rev. Lett. **76**, 2318 (1996).
[15] F. Abraham, D. Brodbeck, R. A. Rafey, and W. Rudge, Phys. Rev. Lett. **73**, 272 (1994).
[16] S. Roux and E. Guyon, J. Phys. (France) Lett. **46**, L999 (1985).
[17] H. J. Herrmann, J. Kertész, and L. de Arcangelis, Europhys. Lett. **10**, 147 (1989).
[18] S. Feng and P. N. Sen, Phys. Rev. Lett. **52**, 216 (1984).
[19] Y. Kantor and I. Webman, Phys. Rev. Lett. **52**, 1891 (1984).
[20] P. M. Duxbury, P. L. Leath, and P. D. Beale, Phys. Rev. B **36**, 367 (1987).
[21] L. de Arcangelis and S. Reder, J. Phys. (France) Lett. **46**, L585 (1985).
[22] A. Hansen, S. Roux, and H. J. Herrmann, J. Phys. (Paris) **50**, 733 (1989).
[23] *Statistical Models for the Fracture of Disordered Media*, edited by H. J. Herrmann and S. Roux (North-Holland, Amsterdam, 1990).
[24] P. Meakin, Thin Solid Films **151**, 165 (1987).
[25] H. Colina, L. de Arcangelis, and S. Roux, Phys. Rev. B **48**, 3666 (1993).
[26] T. L. Anderson, *Fracture Mechanics* (CRC Press, Boca Raton, FL, 1995).
[27] D. M. d. G. Allen, *Relaxation Methods* (McGraw-Hill, New York, 1954).
[28] O. Morgenstern, I. M. Sokolow, and A. Blumen, Europhys. Lett. **22**, 487 (1993).
[29] D. Stauffer and A. Aharony, *Introduction to Percolation Theory* (Taylor and Francis, London, 1992).
[30] F. L. Ladeira and N. J. Price, J. Struct. Geol. **3**, 79 (1981).
[31] Q. Huang and J. Angelier, Geol. Mag. **126**, 355 (1989).
[32] T. Walmann (unpublished).
[33] P. Segall and D. D. Pollard, Bull. Geol. Soc. Am. **94**, 563 (1983).
[34] J. Walsh, J. Watterson, and G. Yielding, Nature (London) **351**, 391 (1991).
[35] K. J. Heffner and T. G. Bevan, SPE J. **20981**, 367 (1990).
[36] J. M. Vermilye and C. H. Scholz, J. Struct. Geol. **17**, 423 (1995).